Applied Physics Letters

Atomic layer deposition of SiO_2–GeO_2 multilayers

Cite as: Appl. Phys. Lett. **117**, 041601 (2020); https://doi.org/10.1063/5.0009844
Submitted: 03 April 2020 . Accepted: 09 July 2020 . Published Online: 28 July 2020

Jordi Antoja-Lleonart, Silang Zhou, Kit de Hond, Sizhao Huang, Gertjan Koster, Guus Rijnders, and Beatriz Noheda

Applied Physics Letters ARTICLE scitation.org/journal/apl

Atomic layer deposition of SiO_2–GeO_2 multilayers

Cite as: Appl. Phys. Lett. **117**, 041601 (2020); doi: 10.1063/5.0009844
Submitted: 3 April 2020 · Accepted: 9 July 2020 ·
Published Online: 28 July 2020

Jordi Antoja-Lleonart,[1,a)] Silang Zhou,[1] Kit de Hond,[2] Sizhao Huang,[2] Gertjan Koster,[2] Guus Rijnders,[2] and Beatriz Noheda[1,b)]

AFFILIATIONS

[1]Zernike Institute for Advanced Materials, University of Groningen, 9747AG Groningen, The Netherlands
[2]MESA+ Institute for Nanotechnology, University of Twente, PO Box 217, 7522 NH Enschede, The Netherlands

[a)]Electronic mail: j.antoja.lleonart@rug.nl
[b)]Author to whom correspondence should be addressed: b.noheda@rug.nl

ABSTRACT

Despite its potential for CMOS applications, atomic layer deposition (ALD) of GeO_2 thin films, by itself or in combination with SiO_2, has not been widely investigated yet. Here, we report the ALD growth of SiO_2/GeO_2 multilayers on si1icon substrates using a so far unexplored Ge precursor. The characterization of multilayers with various periodicities reveals layer-by-layer growth with electron density contrast and the absence of chemical intermixing, down to a periodicity of two atomic layers.

In the last four decades, atomic layer deposition (ALD) has seen widespread adoption as a thin film growth technique.[1,2] Its scalability, unprecedented conformality, and thickness control down to the atomic level make it a valuable asset to most nanofabrication efforts, playing a key role in commercial semiconductor manufacturing. Although chiefly known for the growth of relatively simple compounds, such as binary oxides, nitrides, or sulfides, amorphous for the most part, ALD is also used to grow metals,[3] and recently, more complex, multicomponent materials,[4,5] including perovskites,[6–10] have been realized as well.

One of the materials with the longest history using the ALD techniques is SiO_2,[11] a key element in the microelectronics industry with applications as a passivation layer and gate oxide, among others. Less ubiquitous is the ALD growth of the related material GeO_2; its growth using ALD is relatively unexplored, and not many of its possible precursors have been tested.[12–14] Research on GeO_2 films has been mainly devoted to the study of the GeO_2/Ge interface, with GeO_2 films being proposed as a means to reduce the concentration of interface states between Ge and a high-K dielectric on top,[15–17] with the goal of realizing MOSFETs with a Ge-based channel. In these studies, thermal or plasma oxidation, as well as vapor growth,[18,19] was used. It is worth mentioning that these works use precursors containing alkoxy or halide ligands, which, in SiO_2 ALD, have been shown to have less-than-ideal reactivity and corrosive byproducts.[20,21]

Thin films consisting of SiO_2 and GeO_2 multilayers have been investigated in the past, from both solution and vapor deposition methods,[22–24] with the focus being mostly on their optical properties. In this work, we show that using tetrakis(dimethylamino)germanium (IV) (TDMAGe) as a precursor, it is possible to deposit GeO_2 as well as SiO_2/GeO_2 multilayers by thermal ALD. Proper intermixing between SiO_2 and GeO_2 in ALD multilayers is a key goal of this growth experiment. Achieving intermixing via post-annealing is not an option, given that these two compounds are known to phase separate, rather than mix, upon heating.[25,26]

We use a Picosun R-200 Advanced hot-wall ALD System whose chamber opens to a glovebox containing a nitrogen atmosphere, with controlled oxygen and water concentrations. We grow oxide thin films using organometallic Si and Ge precursors. These are bis(diethylamino)silane (BDEAS, commonly known as SAM-24) and TDMAGe, respectively, both of them purchased from Air Liquide. The precursors are housed in PicohotTM 300 and PicohotTM 200 canisters, which allow heating up to 260 °C and 200 °C, respectively. The organometallic precursors are delivered into the reaction chamber, through heated valve blocks, using nitrogen as carrier gas.

The oxidizer used in this work is ozone, which is produced from an INUSA Ozone Generator using Oxygen 6.0. Our valves allow a minimum opening time of 0.1 s. Accessible process temperatures range from 100 °C to 300 °C, and the typical process pressure is 17 hPa. A temperature of 38 °C for the BDEAS precursor bottle was established to give acceptable delivery rates. The TDMAGe bottle needed to be heated to 80 °C to achieve similar precursor delivery rates to the reaction chamber. The gas lines downstreaming from the bottles

were heated to 10–20 °C above the temperature of their respective bottle to avoid precursor condensation taking place before reaching the reaction chamber.

The SiO_2 growth from BDEAS was optimized in collaboration with Picosun®. The reactor temperature was set to 300 °C. The BDEAS pulse length was 0.1 s, followed by a 6.0 s N_2 purge. The ozone pulse length was 8.0 s, also followed by a 6.0 s N_2 purge. In our system, SiO_2 grown in this way shows a growth per cycle (GPC) of about 0.7 Å. The GeO_2 growth has been independently optimized in the present work, as detailed below. The films are grown on 15 × 15 mm^2 square pieces of Si(100) wafers purchased from Microchemicals GmbH.

Although the growth of GeO_2 by ALD using TDMAGe as a precursor was recently patented,[14] the details of the growth were not reported. Even though the precursors used for GeO_2 and SiO_2 are quite different, both of them use alkylamine ligands. This allowed us to optimize the GeO_2 growth, using as starting parameters those of the SiO_2 growth.

In the case of the combined SiO_2/GeO_2 multilayer growth, there are practical constraints to the process. First, the well-known SiO_2 precursor BDEAS,[27–32] requires ozone or oxygen to function properly in thermal ALD. If water vapor is used instead, the Si–H bonds in the precursor do not react, which results in a decreased growth rate, possibly leading to too high impurity concentrations in the film. For this reason, it is highly desirable to simplify the process by using ozone as the oxidizer in GeO_2 growth as well, even though this may lead to combustion-like reactions and less gentle oxidization. The ozone pulse length was fixed at 8 s, sufficient to ensure a complete half-reaction.

Second, the SiO_2 growth is optimal at or above 300 °C. When growing subsequent layers of different materials by ALD, it is, in principle, possible to change the reaction temperature when switching from one oxide to the next. However, cooling and heating the reactor, even for relatively small temperature differences, are slow processes, making the growth time prohibitively long if the temperature needs to be changed repeatedly. For this reason, while the optimal growth temperature for pure GeO_2 is determined, if GeO_2 growth is still acceptable at 300 °C, this temperature needs to be maintained in the multilayer growth.

The minimum operating temperature of our system is, for this process, about 100 °C. This is necessary to avoid condensation of the precursors or their reaction products in the chamber. Its maximum operating temperature is 300 °C in its current configuration. Within this range, the growth rate of pure GeO_2 increases with increasing temperature, remaining approximately invariant above 150 °C ([Fig. 1(b)]. One explanation for this behavior is that below 150 °C, the chemisorption reaction rate for TDMAGe is too low for proper ALD behavior, resulting in a decreased GPC. It could be argued that the stabilization of the GPC up to 300 °C is an indication that precursor decomposition is still not significant at that temperature.

The GPC dependence on the pulse length was analyzed as well. The purge times were kept constant for this series. We can see that the GPC at 300 °C increases for longer TDMAGe pulses [Fig. 1(d)], while displaying approximately constant values for the short pulse lengths of 0.1 s and 0.2 s. This could indicate that this temperature is, in fact, sufficient to cause noticeable precursor decomposition, but that this has no noticeable effect in the growth, provided that the TDMAGe pulses are short enough. This was confirmed by growing a film at 200 °C

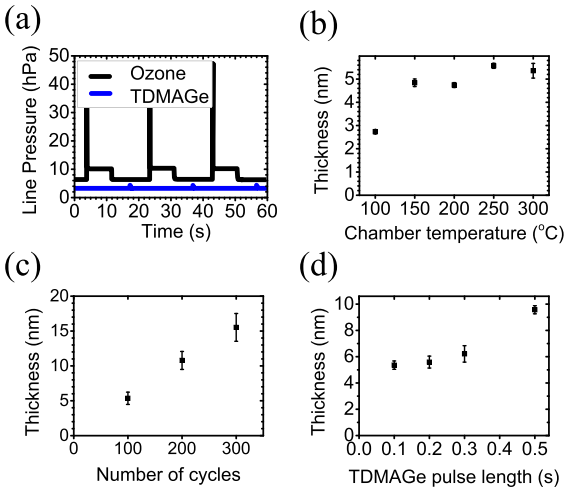

FIG. 1. (a) Sketch of the pulse trains of the two precursors. (b) GeO_2 film thickness after 100 cycles at various reactor temperatures. (c) GeO_2 film thickness for different cycle numbers, at 300 °C. A linear regression for this regime yields a GPC of 0.51 Å. (d) GeO_2 film thickness for 100 cycles and at 300 °C for different TDMAGe pulse lengths. Error bars are estimated based on sample dispersion.

using TDMAGe pulses of 0.5 s. In that case, the GPC was 0.53 Å. This shows that the effect of precursor decomposition on the thickness can be minimized either by growing at sufficiently low temperatures, which is difficult in our case, as discussed before, or by keeping the pulse length short. Therefore, the shortest pulse length of 0.1 s was chosen. We further show, for large pulse numbers, the dependence of the film thickness on the number of pulses [Fig. 1(c)].

The dielectric properties of GeO_2 films grown with the optimized parameters were also investigated. Figure 2 shows the result of several capacitance measurements on one of these films. At low frequencies, we observe a Debye relaxation with a characteristic time of 6 ms, which was determined from fitting the real component of the permittivity (ε_r'). This likely corresponds to space charge relaxation. The relative dielectric constant at 1 kHz is $\varepsilon_r' = 22$.

The dielectric constant value that we have determined at 1 kHz is significantly larger than those available in the literature, such as the

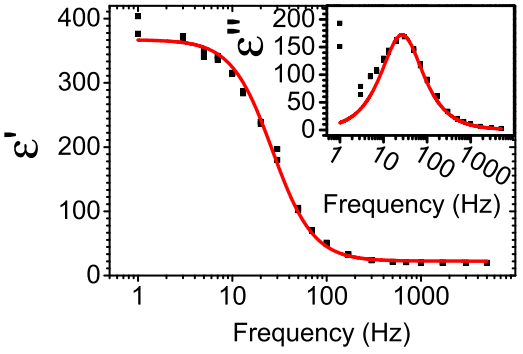

FIG. 2. Relative dielectric constant (real and imaginary) for a 12 nm GeO_2 film as calculated from C–V measurements between 1 Hz and 5 KHz. The tan(δ) value is below 1 for all points above 300 Hz. Dispersion between successive measurements is most visible at low frequencies. The red lines are a Debye fit with $\tau = 6$ ms.

theoretical value of $\varepsilon_r' \sim 2.8$ extrapolated by Walker *et al.*,[33] the experimentally determined static ε_r' between 5 and 7 for GeO_2 grown by Ge oxidization,[34,35] or the near-static value of $\varepsilon_r' \sim 8.5$ for vacuum-evaporated films.[36] Some GeO_2 crystalline phases have also been explored,[37–39] with their ε_r' being significantly different for different phases. We have also determined the dielectric constant by spectroscopic ellipsometry in the range of 300–1700 nm (see the supplementary material). These results reveal a high-frequency $\varepsilon_r' \sim 2$, slightly smaller than literature sources.[40–43] This suggests at least one more relaxation process between 5 kHz and the near-infrared (NIR) range. This relaxation can be of the dipole polarization of small amounts of absorbed water, as GeO_2 is known to be hygroscopic.[44]

We then proceeded to grow multilayer heterostructures with alternating SiO_2 and GeO_2 sublayers. This multilayer approach has been often utilized to synthesize complex materials by ALD.[4] This layered growth is often characterized in the literature by the ratio between the numbers of pulses of the metal precursors of the two components. Here, we have synthesized multilayers with different SiO_2/GeO_2 periodicities using a constant 1:1 pulse ratio and the same total number of pulses (the same total thickness), but varying the number of pulses in each train. In this way, it is possible to control the degree of intermixing during the growth step, without resorting to post-annealing.

For the experiments here, we set the total number of cycles to 300, of which half will be GeO_2 and the other half SiO_2. Note that, assuming that the behavior displayed in Fig. 1(c) can be extrapolated to lower cycle numbers, the expected thickness for the GeO_2 and SiO_2 layers would be 8 nm and 11 nm, respectively, taking into account our previously mentioned GPC values at the optimized process parameters. Thus, assuming an ALD linear regime, we expect a total thickness of 19 nm approximately, without accounting for the native oxide present on the wafer. This is in good agreement with the values obtained from the fitting of the XRR patterns, which give total thicknesses ranging between 19.2 nm and 20.1 nm (see Table S1 in the supplementary material).

The first experiment, with 150 cycles of $TDMAGe/O_3$ followed by 150 cycles of $BDEAS/O_3$, is denoted as "one repetition" (see Fig. 3). One repetition, thus, contains a GeO_2 sublayer and a SiO_2 sublayer. In the following experiments, the number of cycles in each sublayer is subsequently halved, while the number of repetitions is doubled in order to keep the total number of pulses constant. The XRR patterns of these films, their fits and an illustration of the models used in the fits, are plotted in Fig. 4 (the actual parameters of the model can be found in Table S1 of the supplementary material). By differentiating the experimental data (which has been obtained with a step size of 0.01° in 2θ) at low angles and smoothing it with a Savitzky–Golay filter, we determined the critical angle for all the films to be 0.235° ± 0.005°, independent of the number of repetitions (or the periodicity of the multilayer), close to the bulk value for SiO_2 (0.234° for a density of 2.65 g/cm^3).

The XRR patterns show clear thickness oscillations in all cases, indicating the good homogeneity of the films and the quality of the top and bottom interfaces. In addition, the patterns corresponding to the films containing from 2 up to 15 repetitions all display superlattice reflections, attesting for the presence of chemical contrast between the SiO_2 and GeO_2 sublayers.

The XRR pattern of the film with 15 repetitions shows its superlattice signature peak at about 7.1°, corresponding to a period of 12 Å,

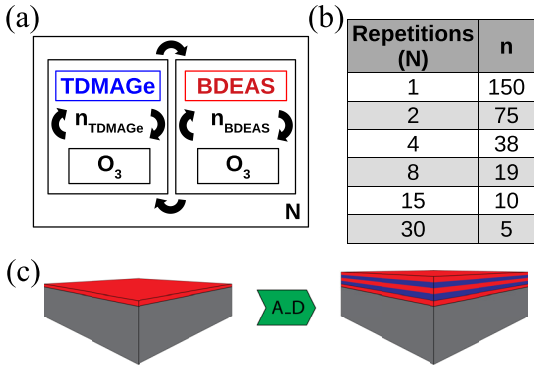

Repetitions (N)	n
1	150
2	75
4	38
8	19
15	10
30	5

FIG. 3. (a) Schematic representation of the synthesis method for the mixed oxide films. In our study, the pulse trains for the two precursors contain the same number of pulses: $n_{TDMAGe} = n_{BDEAS} = n$, and it varies from film to film. (b) Table detailing the number of precursor pulses in each train (n) per sublayer and the total number of cycles (N) in the different films. For the 1:1 pulse ratio used in this work, the total number of cycles ($2n \times N$) was kept to approximately 300 for the whole series. This means that for the 1 repetition case, 150 cycles of $TDMAGe/O_3$ were done, and after that came 150 cycles of $BDEAS/O_3$, for a total of 300 cycles in two layers. (c) Sketch of the expected layered structure after growth.

which is approximately the size of two unit cells in SiO_2 and GeO_2 crystalline polymorphs. In the case of the 15 repetitions sample, despite the clear superlattice peak, the model is not able to provide a reliable value for the thickness of the individual SiO_2 or GeO_2 sublayers. This can be understood looking at the roughness values (see Table S1 in the supplementary material), which are of the order of the estimated sublayer thickness (6 Å). For the 30 repetition film, only 5 pulses were provided, alternately, for each SiO_2 and GeO_2 sublayer, until the total of 300 pulses is complete. Therefore, the superlattice periodicity is expected to be half of the value of the periodicity displayed by the 15 repetition films, 6 Å. This value is similar to the

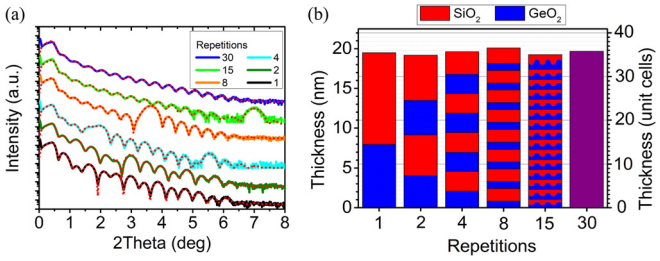

FIG. 4. (a) XRR scans and fits (red dashed lines) of the six films, from which the thicknesses were extracted. (b) Side view of the grown films, showing the actual layer thicknesses as determined by XRR. The red and blue stripes indicate layers made of different oxides, whereas the purple stripe is used for a layer of mixed oxide. Superlattice fits add the constraint that all SiO_2 layers and all GeO_2 layers in a single heterostructure have the same thickness, but this constraint is relaxed for the top SiO_2 and the bottom GeO_2 layer in each case, respectively. The native SiO_2 layers, although both measured by ellipsometry prior to the ALD process and accounted for in the models, are not depicted here. Note that the models do include interface roughnesses. The right axis shows the thickness in multiples of 0.55 nm, which is approximately the average between the SiO_2 and GeO_2 α-quartz of the c-parameter, as it is used as a characteristic length scale of the material (though it is amorphous in this case).

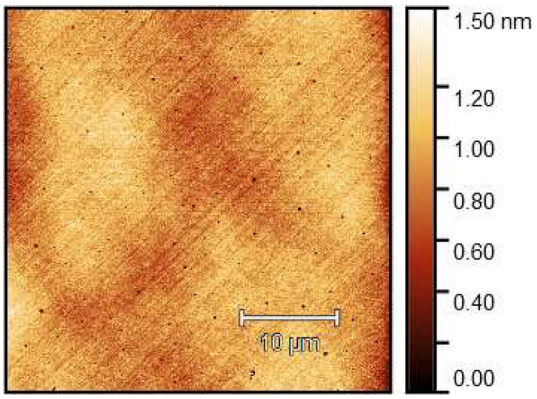

FIG. 5. Representative AFM image, corresponding to a two-repetition sample.

roughness values obtained with the reflectivity fit, and thus, no chemical contrast is expected. Indeed, in this case, the superlattice model also gives unreliable results, but, unlike in the case of the 15 repetition film, the 30 repetition XRR pattern can be modeled by a uniform layer (see Table S1 in the supplementary material), consistent with the absence of superlattice peaks up to an angle of 14°.

The model roughness values are in agreement with those determined by AFM (RMS roughness). Figure 5 shows a representative AFM image of a sample surface. AFM micrographs of the six multilayer types are available in the supplementary material, as are the AFM roughnesses, in Table S1. In addition, x-ray Photoelectron Spectroscopy (XPS) on these films has shown small amounts of carbon contamination in the films (see the supplementary material), most likely arising from the ALD growth process.

From this series of experiments, it becomes clear that electron density, or composition, contrast between the SiO_2 and the GeO_2 sublayers is present down to the atomic level (close to a unit cell of their stable polymorphs). On the one hand, these results attest the excellent capabilities of ALD in general, allowing the growth of heterostructures with atomic-scale thickness control. On the other hand, it nicely illustrates a potential pitfall of the layered approach to compositional tuning in ALD, in that extremely short supercycles are needed in order to achieve a uniform composition rather than a superlattice.

As a final note, it must be pointed out that, as directly visible in Fig. 4, the SiO_2:GeO_2 thickness ratio, and therefore the atomic ratio, changes from one film to the next, even though the pulse ratio for all of them is maintained at 1:1. This dependence of the composition on the precise pulsing sequence, and not only on the pulse ratio, has been previously observed.[45]

To conclude, we have optimized the ALD growth of GeO_2 thin films from TDMAGe and O_3 precursors. In order to achieve SiO_2/GeO_2 films by sequential layered growth, a compromise has been found between the optimal growth parameters and those parameters that will allow us to synthesize a mixed oxide film in a reasonable amount of time. Armed with this knowledge, we have set out on the synthesis of a series of increasingly intermixed SiO_2/GeO_2 thin films, showing that ALD indeed is able to achieve atomic level accuracy for these compounds as well.

See the supplementary material for further details on the experimental methods, high-frequency ellipsometry-determined dielectric constants, AFM images of the films, and details and fitting parameters giving rise to the XRR simulation curves in Fig. 4.

The authors are grateful to Picosun® for their optimization report related to the growth of SiO_2, to Adrian Carretero-Genevrier and Václav Ocelík for useful discussions, and to Ir. Jacob Baas and the Zernike NanoLab Groningen for the technical support. The authors also acknowledge financial support from NWO's TOP-PUNT Grant No. 718.016002.

DATA AVAILABILITY

The data that support the findings of this study are available from the corresponding author upon reasonable request.

REFERENCES

[1]R. L. Puurunen, J. Appl. Phys. **97**, 121301 (2005).
[2]R. W. Johnson, A. Hultqvist, and S. F. Bent, Mater. Today **17**, 236 (2014).
[3]J. Hämäläinen, M. Ritala, and M. Leskelä, Chem. Mater. **26**, 786 (2014).
[4]A. J. Mackus, J. R. Schneider, C. Macisaac, J. G. Baker, and S. F. Bent, Chem. Mater. **31**, 1142 (2019).
[5]M. Coll and M. Napari, APL Mater. **7**, 110901 (2019).
[6]M. Tyunina, M. Plekh, J. Levoska, M. Vehkamäki, M. Hatanpää, M. Ritala, and M. Leskelä, Integr. Ferroelectr. **102**, 29 (2008).
[7]N. M. Sbrockey, M. Luong, E. M. Gallo, J. D. Sloppy, G. Chen, C. R. Winkler, S. H. Johnson, M. L. Taheri, G. S. Tompa, and J. E. Spanier, J. Electron. Mater. **41**, 819 (2012).
[8]A. R. Akbashev, G. Chen, and J. E. Spanier, Nano Lett. **14**, 44 (2014).
[9]M. D. McDaniel, T. Q. Ngo, S. Hu, A. Posadas, A. A. Demkov, and J. G. Ekerdt, Appl. Phys. Rev. **2**, 041301 (2015).
[10]E. L. Lin, A. B. Posadas, L. Zheng, J. E. Ortmann, S. Abel, J. Fompeyrine, K. Lai, A. A. Demkov, and J. G. Ekerdt, J. Appl. Phys. **126**, 064101 (2019).
[11]Note1. Occasionally "pulsed metal organic chemical vapor deposition" is used instead of ALD, though in practice both methods are very similar.
[12]P. R. Chalker, P. A. Marshall, P. J. King, K. Dawson, S. Romani, P. A. Williams, J. Ridealgh, and M. J. Rosseinsky, J. Mater. Chem. **22**, 12824 (2012).
[13]V. Adinolfi, L. Cheng, M. Laudato, R. C. Clarke, V. K. Narasimhan, S. Balatti, S. Hoang, and K. A. Littau, ACS Nano **13**, 10440 (2019).
[14]R. H. Matero, "Atomic layer deposition of GeO_2 (US Patent)" 2014/0065841 A1 (2014).
[15]T. Yoshida, K. Kato, S. Shibayama, M. Sakashita, N. Taoka, W. Takeuchi, O. Nakatsuka, and S. Zaima, Jpn. J. Appl. Phys., Part 1 **53**, 08LD03 (2014).
[16]S. Shibayama, T. Yoshida, K. Kato, M. Sakashita, W. Takeuchi, N. Taoka, O. Nakatsuka, and S. Zaima, Appl. Phys. Lett. **106**, 062107 (2015).
[17]M. Kanematsu, S. Shibayama, M. Sakashita, W. Takeuchi, O. Nakatsuka, and S. Zaima, Jpn. J. Appl. Phys., Part 1 **55**, 08PC05 (2016).
[18]H. Matsubara, T. Sasada, M. Takenaka, and S. Takagi, Appl. Phys. Lett. **93**, 032104 (2008).
[19]J. Robertson and R. M. Wallace, Mater. Sci. Eng., R **88**, 1 (2015).
[20]J. Bachmann, R. Zierold, Y. T. Chong, R. Hauert, C. Sturm, R. Schmidt-Grund, B. Rheinländer, M. Grundmann, U. Gösele, and K. Nielsch, Angew. Chem., Int. Ed. **47**, 6177 (2008).
[21]M. Putkonen, M. Bosund, O. M. E. Ylivaara, R. L. Puurunen, L. Kilpi, H. Ronkainen, S. Sintonen, S. Ali, H. Lipsanen, X. Liu, E. Haimi, S. P. Hannula, T. Sajavaara, I. Buchanan, E. Karwacki, and M. Vähä-Nissi, Thin Solid Films **558**, 93 (2014).
[22]Q. Y. Zhang, K. Pita, C. K. F. Ho, N. Q. Ngo, L. P. Zuo, and S. Takahashi, Chem. Phys. Lett. **368**, 183 (2003).
[23]C. K. F. Ho, H. S. Djie, K. Pita, N. Q. Ngo, and C. H. Kam, Electromech. Solid-State Lett. **7**, F96 (2004).
[24]C. K. F. Ho, K. Pita, N. Q. Ngo, and C. H. Kam, Opt. Express **13**, 1049 (2005).

[25]H. Hosono and J. Nishii, Opt. Lett. **24**, 1352 (1999).
[26]K. Sasan, A. Lange, T. D. Yee, N. Dudukovic, D. T. Nguyen, M. A. Johnson, O. D. Herrera, J. H. Yoo, A. M. Sawvel, M. E. Ellis, C. M. Mah, R. Ryerson, L. L. Wong, T. Suratwala, J. F. Destino, and R. Dylla-Spears, ACS Appl. Mater. Interfaces **12**, 6736 (2020).
[27]S.-J. Won, S. Suh, M. S. Huh, and H. J. Kim, IEEE Electron Device Lett. **31**, 857 (2010).
[28]M. L. O'Neill, H. R. Bowen, A. Derecskei-Kovacs, K. S. Cuthill, B. Han, and M. Xiao, Electrochem. Soc. Interface **20**, 33 (2011).
[29]S. B. Baek, D. H. Kim, and Y. C. Kim, Appl. Surf. Sci. **258**, 6341 (2012).
[30]A. Mallikarjunan, H. Chandra, M. Xiao, X. Lei, R. M. Pearlstein, H. R. Bowen, M. L. O'Neill, A. Derecskei-Kovacs, and B. Han, J. Vac. Sci. Technol., A **33**, 01A137 (2015).
[31]G. Fang, L. Xu, J. Ma, and A. Li, Chem. Mater. **28**, 1247 (2016).
[32]M. C. Schwille, T. Schössler, F. Schön, M. Oettel, and J. W. Bartha, J. Vac. Sci. Technol., A **35**, 01B119 (2017).
[33]B. Walker, C. C. Dharmawardhana, N. Dari, P. Rulis, and W. Y. Ching, J. Non-Cryst. Solids **428**, 176 (2015).
[34]F. Bellenger, M. Houssa, A. Delabie, T. Conard, M. Caymax, M. Meuris, K. D. Meyer, and M. Heyns, ECS Trans. **11**, 451 (2019).
[35]S. Takagi, T. Maeda, N. Taoka, M. Nishizawa, Y. Morita, K. Ikeda, Y. Yamashita, M. Nishikawa, H. Kumagai, R. Nakane, S. Sugahara, and N. Sugiyama, Microelectron. Eng. **84**, 2314 (2007).
[36]I. Banu Lucy, J. Mater. Sci. **42**, 5875 (2007).
[37]D. M. Roessler and W. A. Albers, J. Phys. Chem. Solids **33**, 293 (1972).
[38]C. Sevik and C. Bulutay, J. Mater. Sci. **42**, 6555 (2007).
[39]M. Tamura, J. Nakamura, and A. Natori, Key Eng. Mater. **470**, 60 (2011).
[40]J. W. Fleming, Appl. Opt. **23**, 4486 (1984).
[41]T. N. Nunley, N. S. Fernando, N. Samarasingha, J. M. Moya, C. M. Nelson, A. A. Medina, and S. Zollner, J. Vac. Sci. Technol., B **34**, 061205 (2016).
[42]G. G. Devyatykh, E. M. Dianov, N. S. Karpychev, S. M. Mazavin, V. M. Mashinskiĭ, V. B. Neustruev, A. V. Nikolaĭchik, A. M. Prokhorov, A. I. Ritus, N. I. Sokolov, and A. S. Yushin, Sov. J. Quantum Electron. **10**, 900 (1980).
[43]L. Pajasová, Czech. J. Phys. **19**, 1265 (1969).
[44]S. R. Da Silva, G. K. Rolim, G. V. Soares, I. J. Baumvol, C. Krug, L. Miotti, F. L. Freire, M. E. Da Costa, and C. Radtke, Appl. Phys. Lett. **100**, 191907 (2012).
[45]V. Longo, N. Leick, F. Roozeboom, and W. M. M. Kessels, ECS J. Solid State Sci. Technol. **2**, N15 (2013).